Figures and figure supplements

Longitudinal fundus imaging and its genome-wide association analysis provide evidence for a human retinal aging clock

Sara Ahadi *et al*.

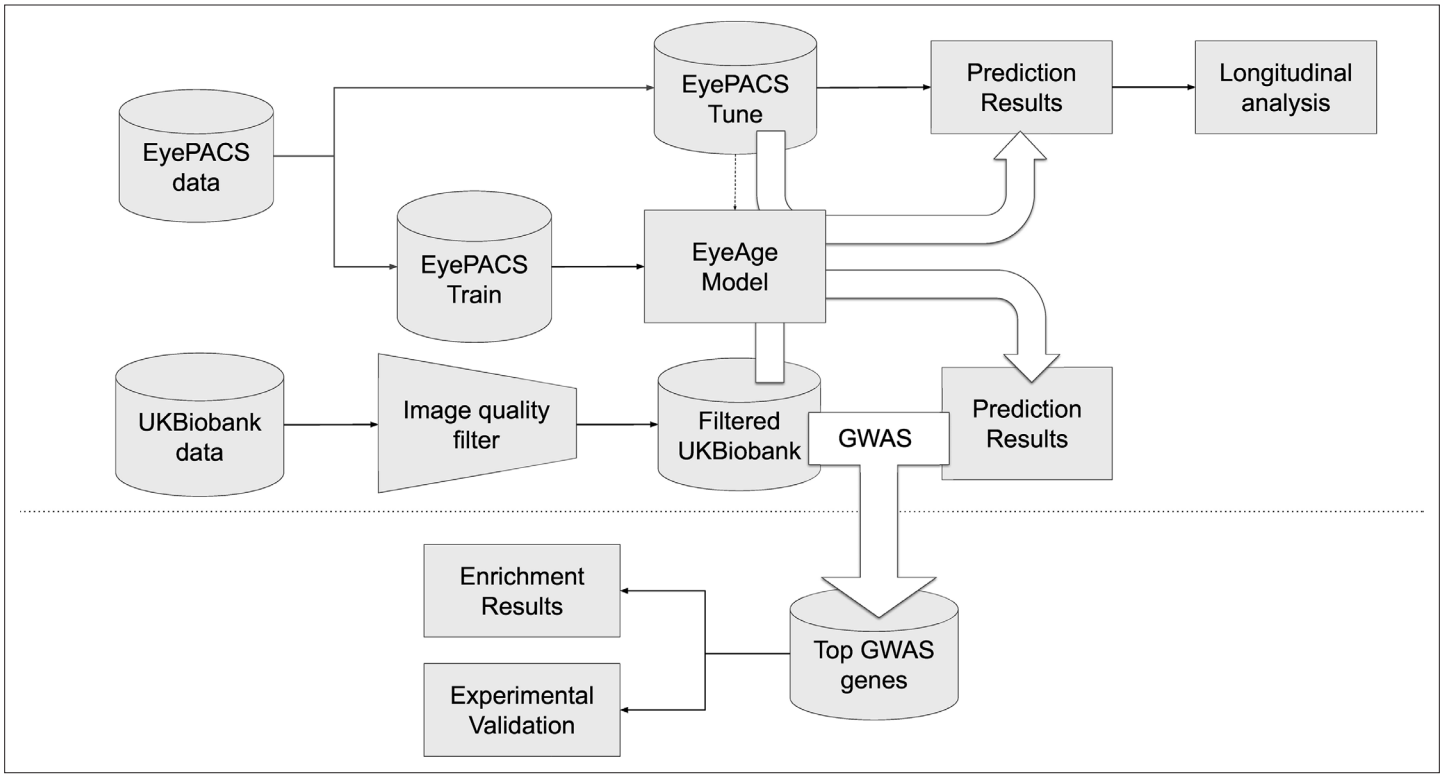

Figure 1. Schematic of analysis pipeline. EyePACS images were split into train and tune sets based on the patient. The model was then trained with the final model step being selected via the tune set. Prediction results on the EyePACS tune set were used for longitudinal analysis of aging. After filtering for image quality, inference was performed with the same model on the UK Biobank dataset and filtering for image quality, and the resulting eyeAgeAccel was used for GWAS analysis. Enrichment analysis was performed on the GWAS hits with a homolog of the top gene (*ALKAL2*) validated experimentally in *Drosophila*.

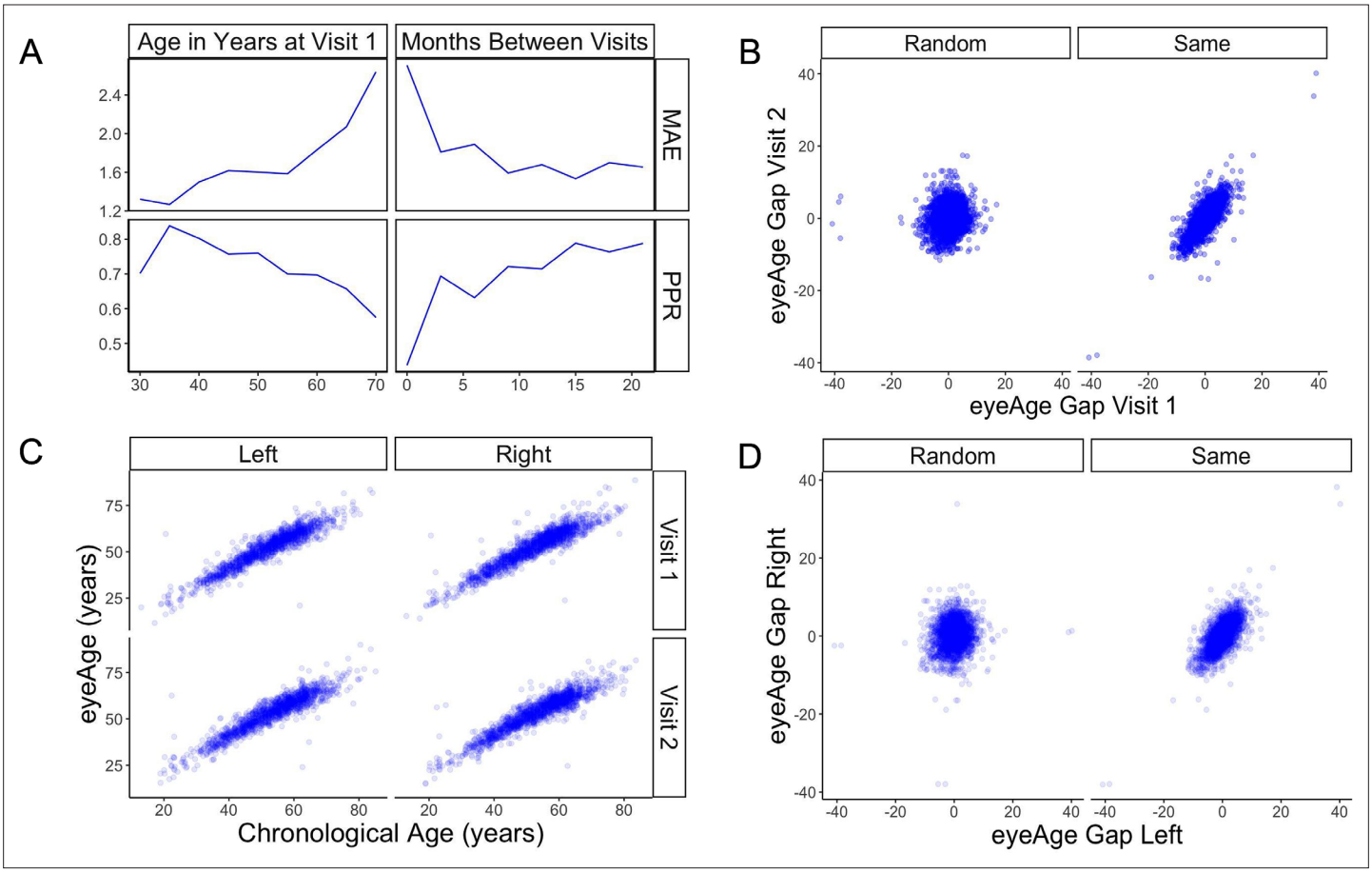

Figure 2. Longitudinal analysis of patients with exactly two visits in the EyePACS cohort. (**A**) Changes of PPR (positive prediction ratio: the ratio of data whose eyeAge increased between subsequent visits) and MAE (mean absolute error) calculated on the same individual in relationship to chronological age at the first visit (left) and time between longitudinal visits (right). (**B**) Scatter plots representing correlation between eyeAge Gap (difference between predicted age and chronological age) of two consecutive visits from an individual (Same) or two consecutive visits from two different individuals (Random). (**C**) Correlation of eyeAge and chronological age between left and right and two consecutive visits of the same individual. (**D**) Scatter plots representing the correlation of left and right eyeAge Gap from the same or two random individuals.

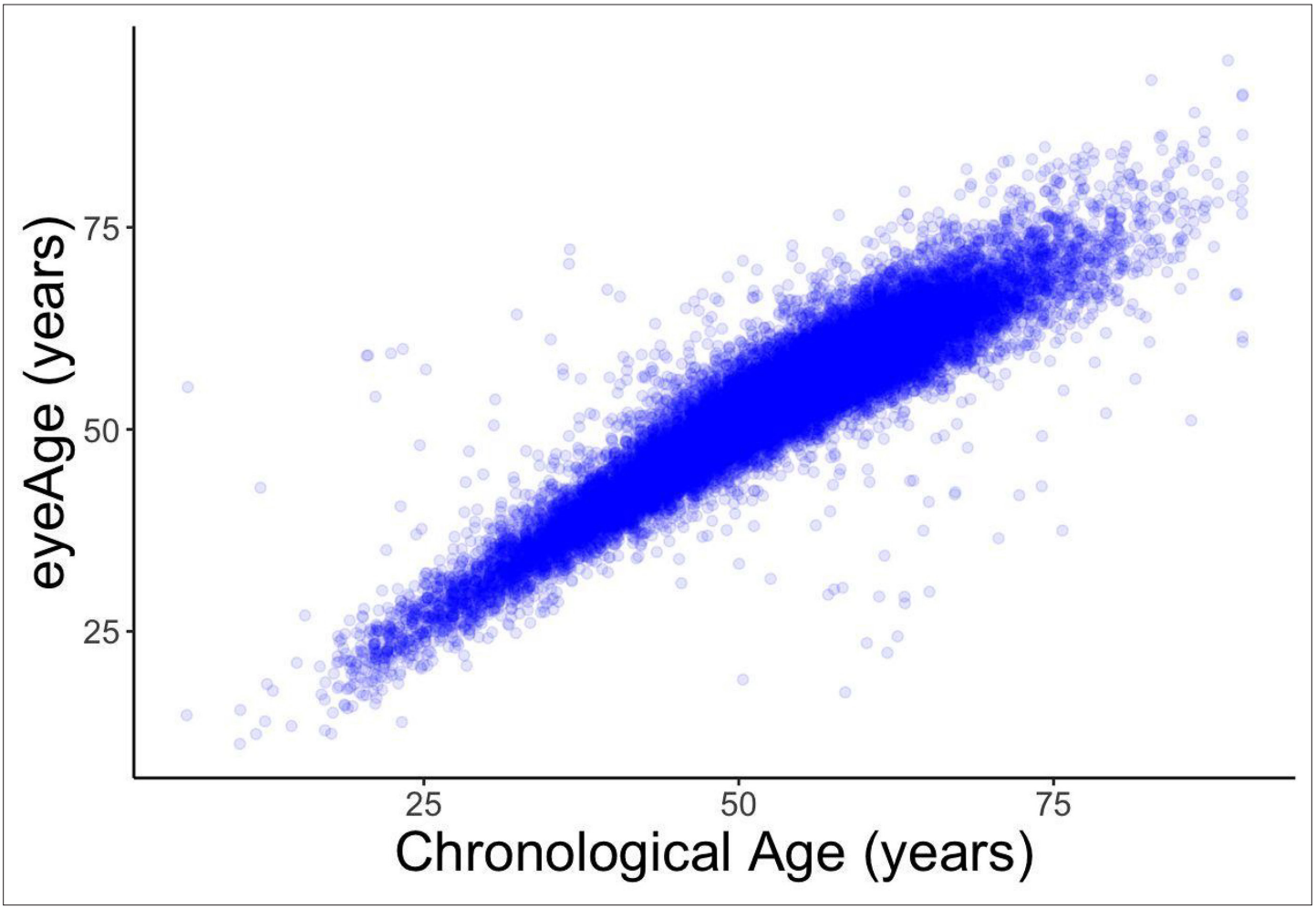

Figure 2—figure supplement 1. Scatter plot of eyeAge with chronological age (Pearson ρ=0.96).

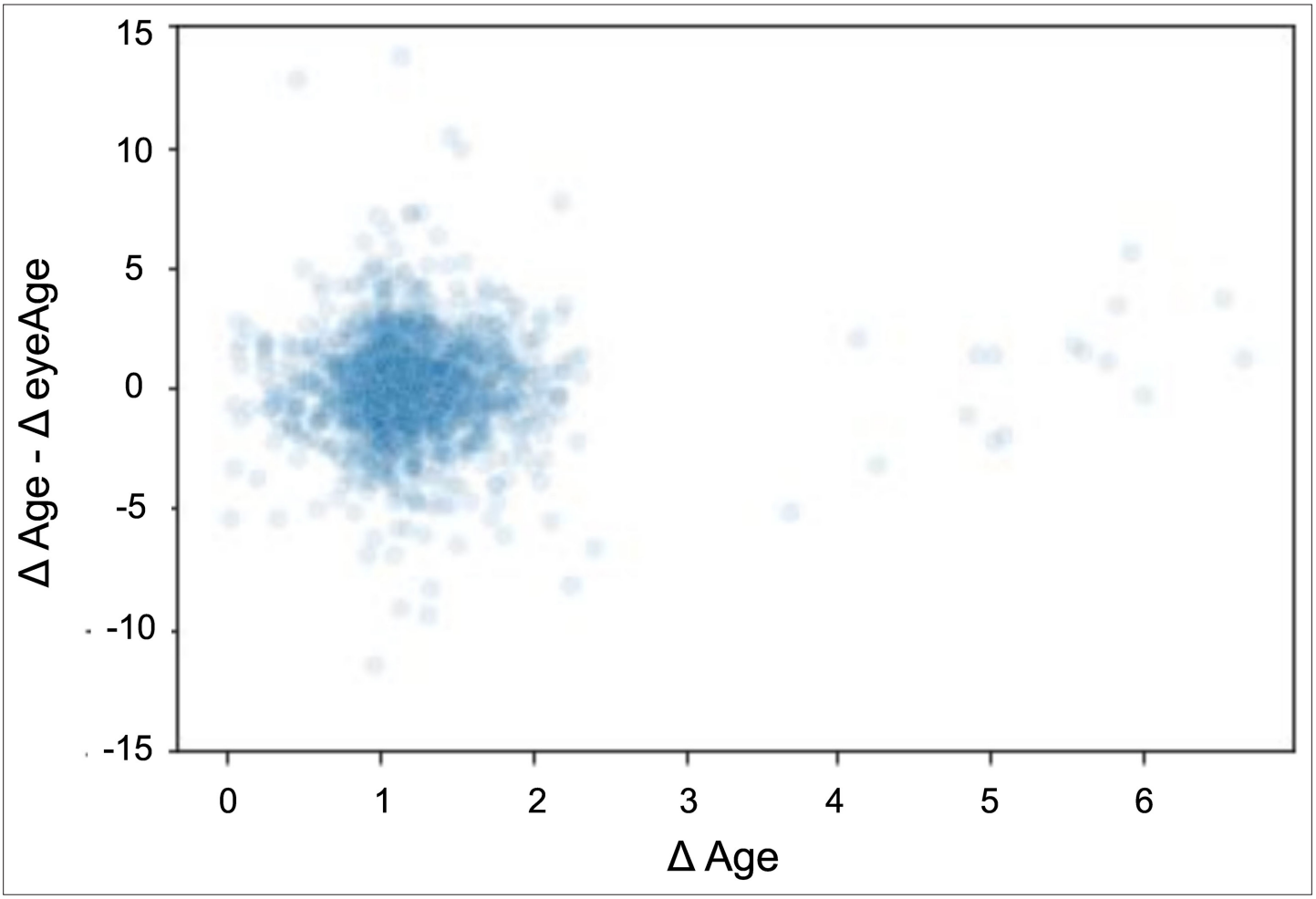

Figure 2—figure supplement 2. Scatterplot showing the time elapsed (x-axis) vs. the difference between time elapsed and change in eyeAge (y-axis).

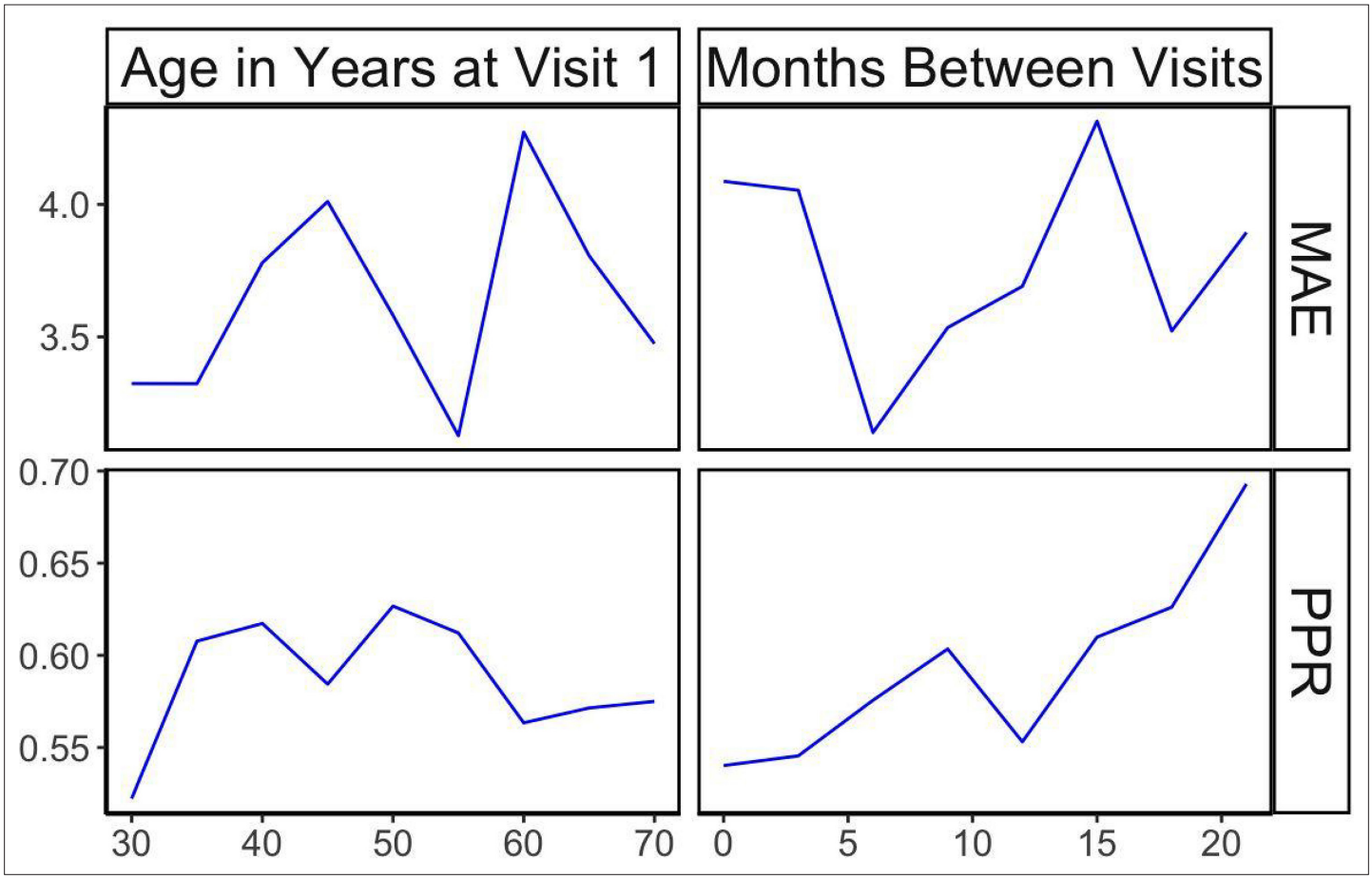

Figure 2—figure supplement 3. Positive prediction ratio and MAE for random, time-matched individuals. Plots shown in relationship to chronological age (left) and time between longitudinal visits (right).

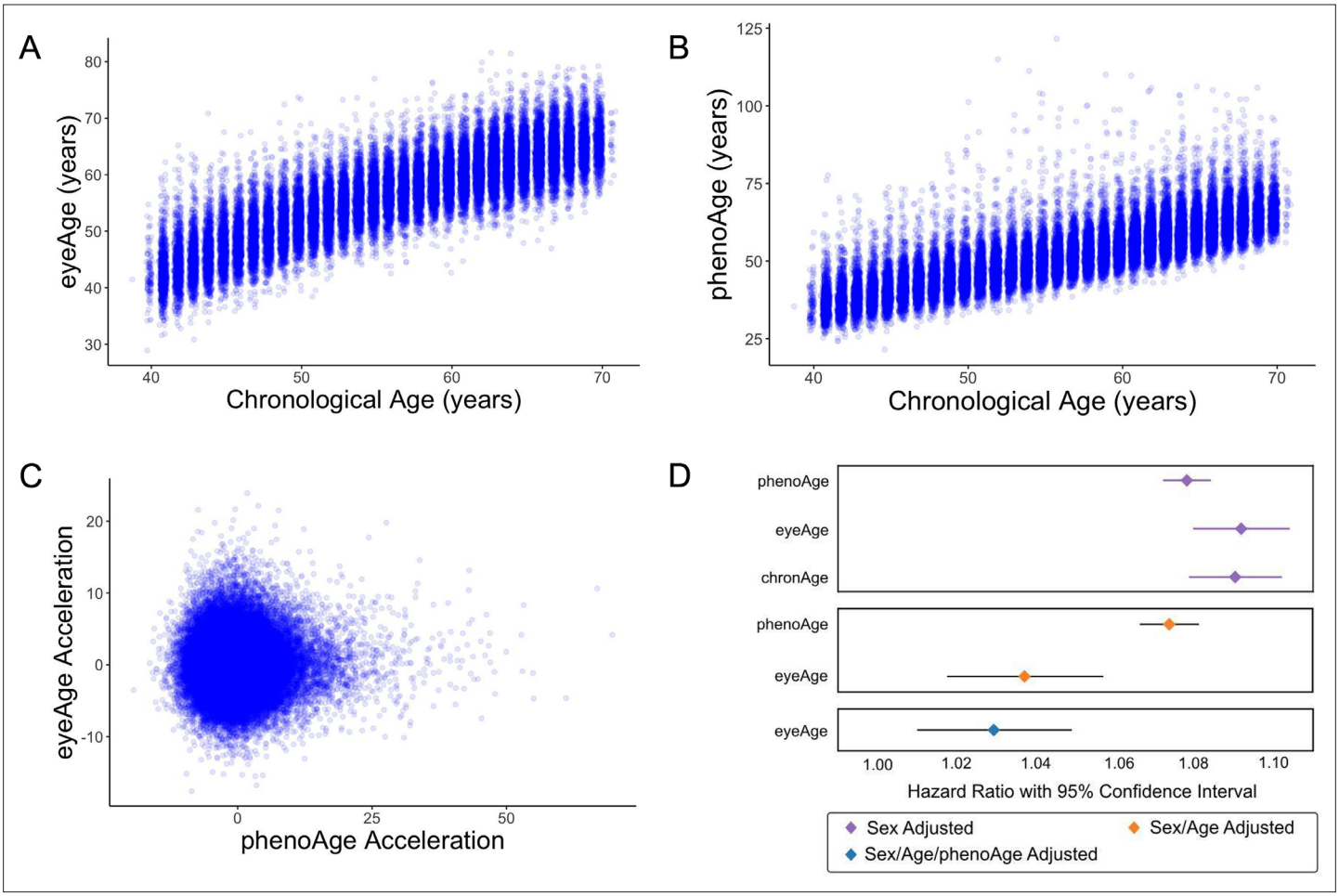

Figure 3. Relationships between eyeAge, phenoAge, and chronological age in the UK Biobank cohort. (**A**) Correlation between eyeAge and chronological age (Pearson ρ=0.86). (**B**) Correlation between phenoAge and chronological age (Pearson ρ=0.82). (**C**) Correlation between eyeAgeAcceleration and phenoAgeAcceleration (Pearson ρ=0.12). (**D**) Forest plot of all-cause mortality hazard ratios (diamonds) and confidence intervals (lines) for the UK Biobank dataset. Purple lines are adjusted only for sex; orange lines are adjusted for sex and age; blue lines are adjusted for sex, age, and phenoAge.

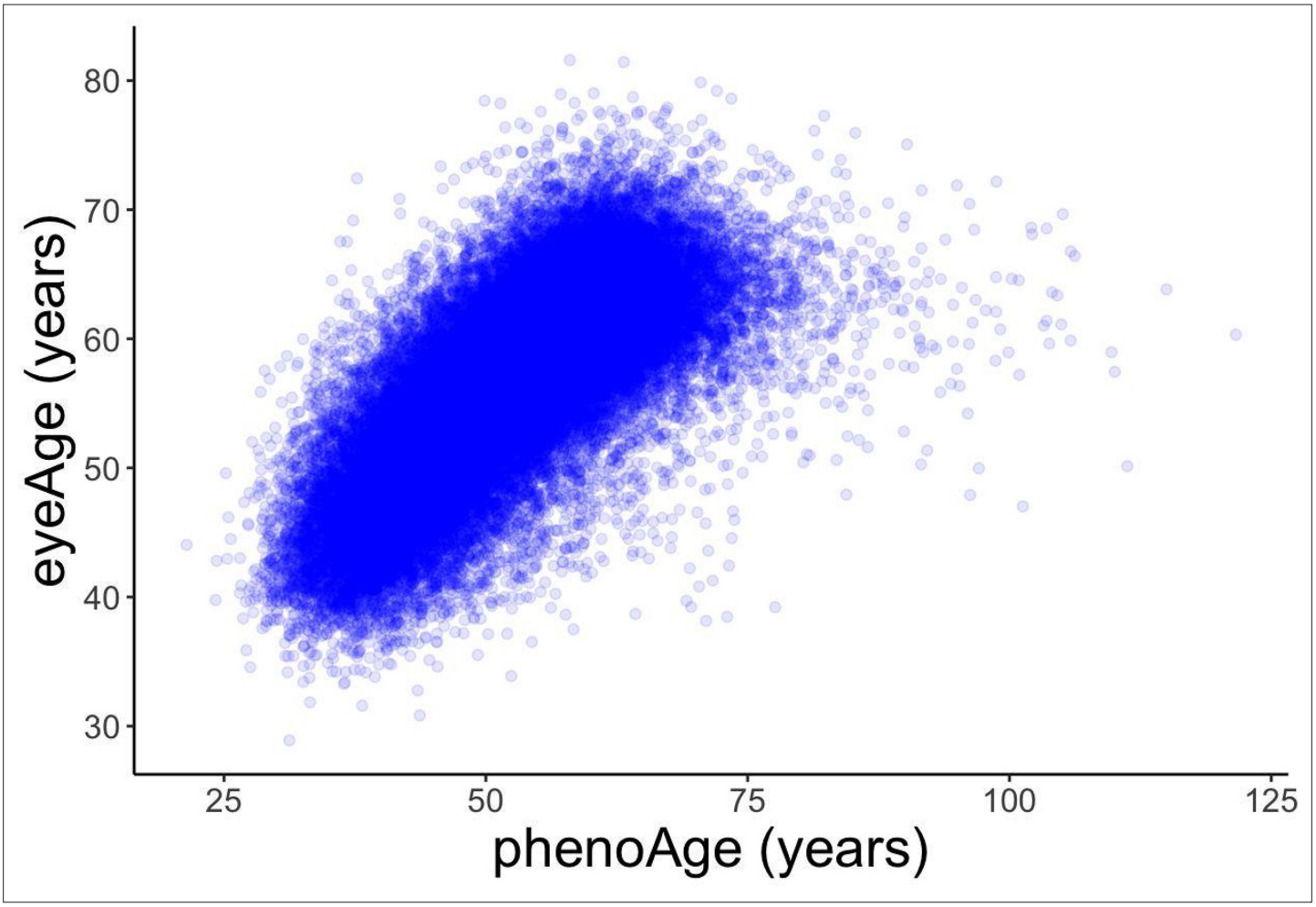

Figure 3—figure supplement 1. Scatter plot of eyeAge and phenoAge (Pearson ρ=0.71).

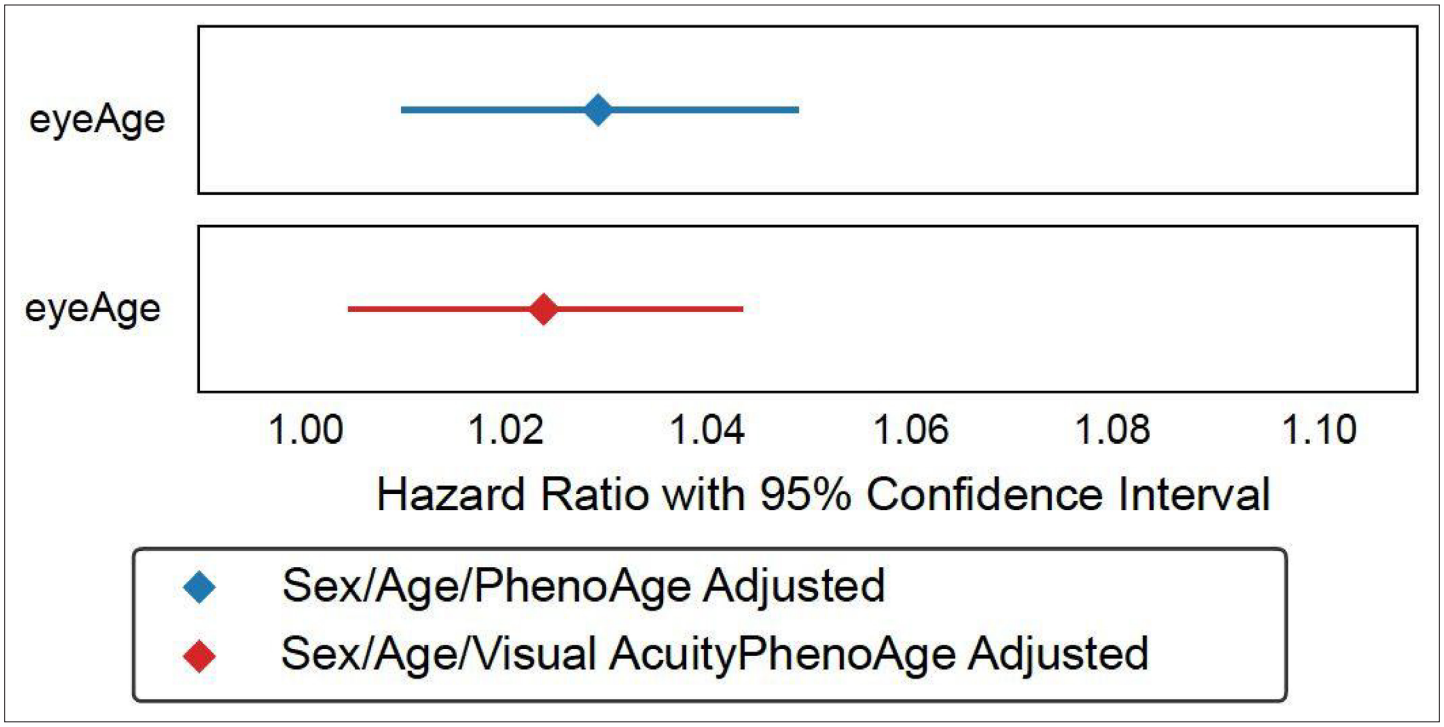

Figure 3—figure supplement 2. eyeAge hazard ratio adjusted with and without visual acuity.

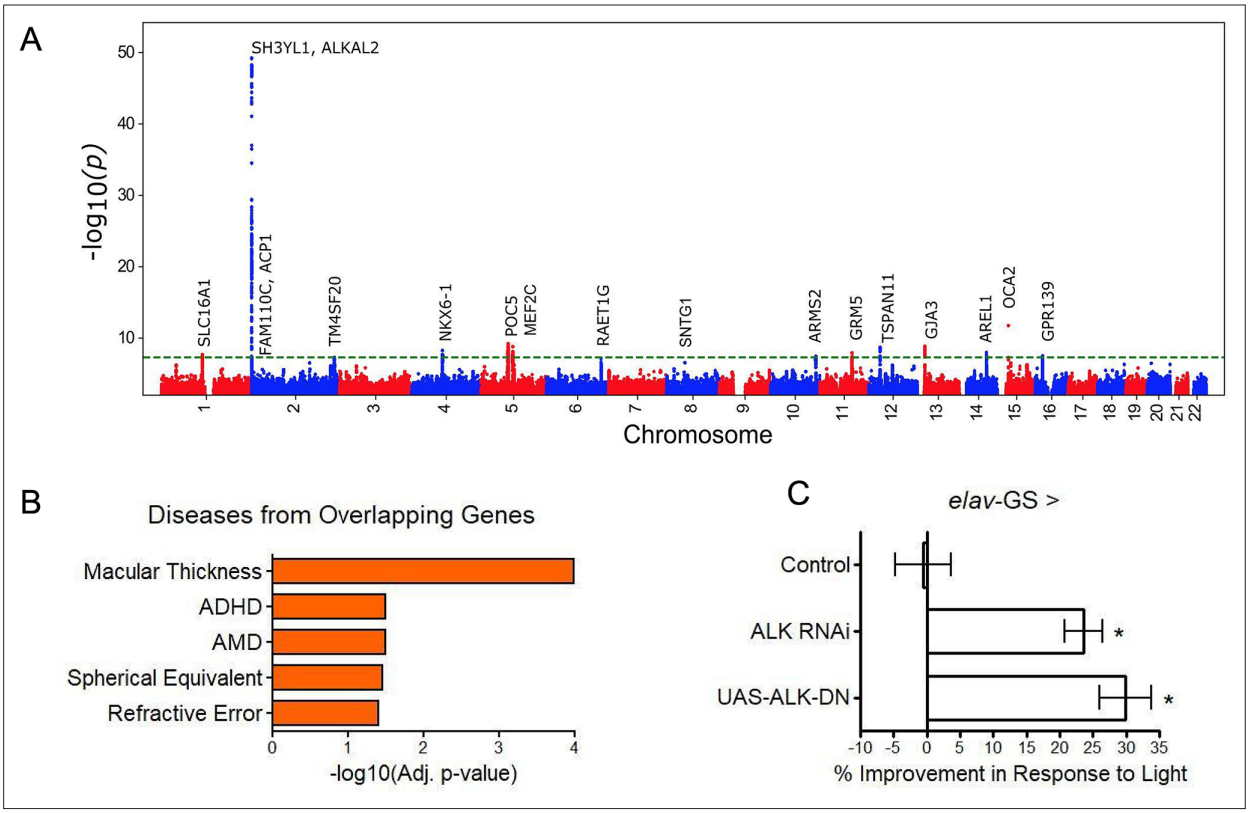

Figure 4. GWAS analyses and experimental validation. (**A**) Manhattan plot representing significant genes associated with eyeAgeAcceleration. (**B**) p-Values for enriched pathways: Macular thickness, ADHD (attention deficit hyperactivity disorder), AMD (age-related macular degeneration), spherical equivalent, and refractive error. (**C**) Assessment of visual performance of transgenic and control flies with age. p-Value is relative to control (*=p < 0.05). p-Value for ALK RNAi vs. control is 0.009; p-value for UAS-ALK-DN vs. control is 0.006. Error bars show standard deviation between 3 biological replicates. n = 100 flies per replicate.

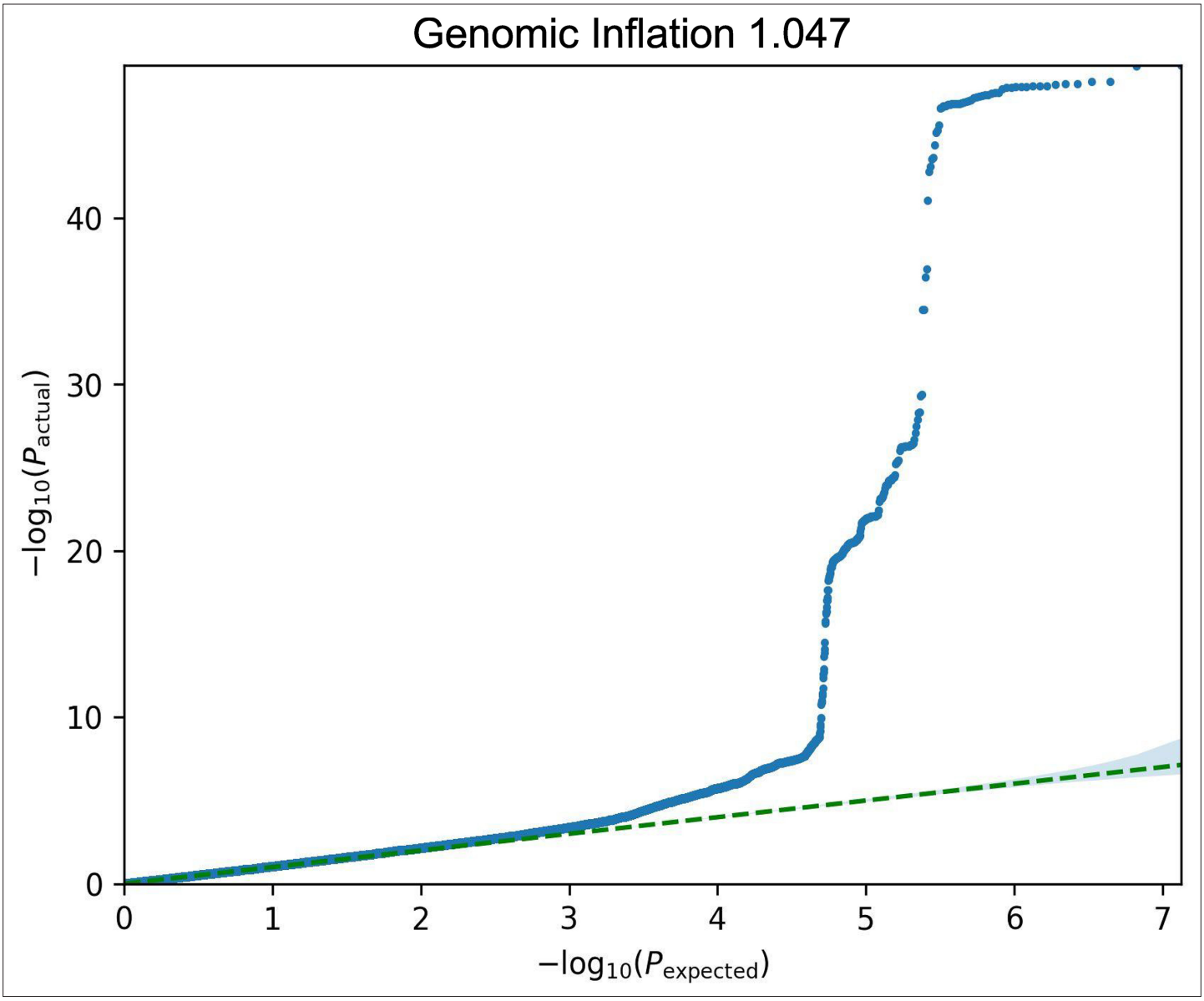

Figure 4—figure supplement 1. eyeAgeAcceleration qq-plot.

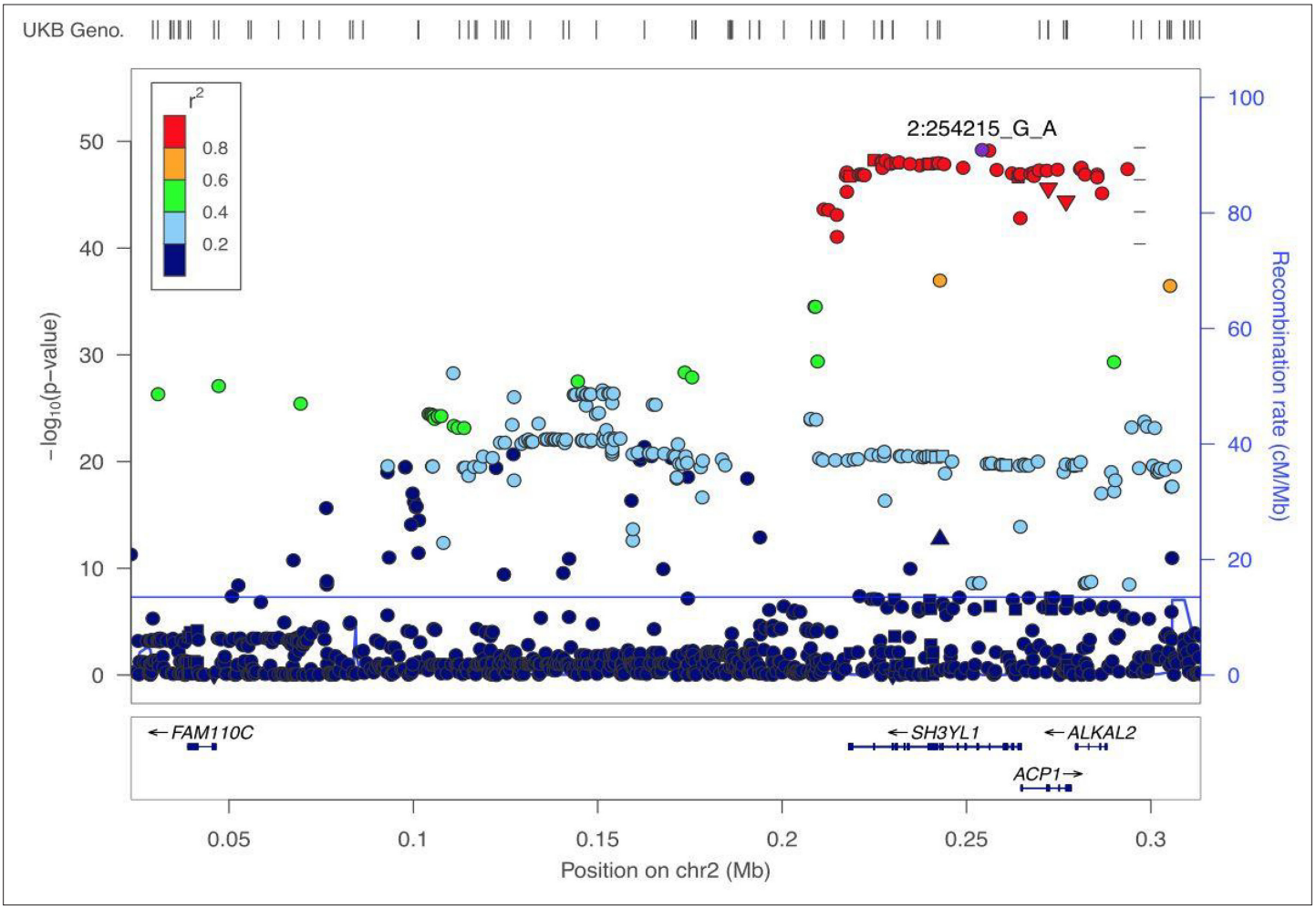

Figure 4—figure supplement 2. Zoom in on significant locus covering three genes in a highly significant LD block. This block includes the three genes: *SH3YL1*, *ACP1*, and *ALKAL2*.